View metadata, citation and similar papers at core.ac.uk

brought to you by CORE

provided by Explore Bristol Research

Knight, M., Damion, R., & Kauppinen, R. (2018). Observation of Angular Dependence of T1 in the Human White Matter at 3T. *Biomedical Spectroscopy and Imaging*. https://doi.org/10.3233/BSI-180183

Peer reviewed version

License (if available):
CC BY-NC

Link to published version (if available):
10.3233/BSI-180183

Link to publication record in Explore Bristol Research

PDF-document

This is the accepted author manuscript (AAM). The final published version (version of record) is available online via IOS at https://doi.org/10.3233/BSI-180183 . Please refer to any applicable terms of use of the publisher.

University of Bristol - Explore Bristol Research

General rights

This document is made available in accordance with publisher policies. Please cite only the published version using the reference above. Full terms of use are available:
http://www.bristol.ac.uk/pure/about/ebr-terms

Observation of Angular Dependence of T1 in the Human White Matter at 3T

Michael J. Knight, Robin A. Damion and Risto A. Kauppinen

School of Psychological Science, University of Bristol, Bristol, BS8 1TU, UK

Corresponding author: Professor Risto Kauppinen
School of Psychological Science
University of Bristol
12a Priory Road
Bristol BS8 1TU, UK
psrak@bristol.ac.uk
Tel + 44 117 928 8461

Running title: Angular dependency of T1 in white matter

ABSTRACT

Background and objective: Multiple factors including chemical composition and microstructure influence relaxivity of tissue water *in vivo.* We have quantified T1 in the human white mater (WM) together with diffusion tensor imaging to study a possible relationship between water T1, diffusional fractional anisotropy (FA) and fibre-to-field angle.

Methods: An inversion recovery (IR) pulse sequence with 6 inversion times for T1 and a multi-band diffusion tensor sequence with 60 diffusion sensitizing gradient directions for FA and the fibre-to-field angle θ (between the principal direction of diffusion and B_0) were used at 3 Tesla in 40 healthy subjects. T1 was assessed using the method previously applied to anisotropy of coherence lifetime to provide a heuristic demonstration as a surface plot of T1 as a function of FA and the angle θ.

Results: Our data show that in the WM voxels with FA > 0.3 T1 becomes longer (i.e. 1/T1 = R1 slower) when fibre-to-field angle is 50-60°, approximating the magic angle of 54.7°. The longer T1 around the magic angle was found in a number of WM tracts independent of anatomy. S0 signal intensity, computed from IR fits, mirrored that of T1 being greater in the WM voxels when the fibre-to-field angle was 50-60°.

Conclusions: The current data point to fibre-to-field-angle dependent T1 relaxation in WM as an indication of effects of microstructure on the longitudinal relaxation of water.

Keywords: Longitudinal relaxation time, relaxation anisotropy, white matter

1. INTRODUCTION

In isotropic liquids, irrespective of any internal molecular motions, fast isotropic rotational diffusion removes any angular dependence, i.e. relaxation is isotropic. An “isotropic liquid” is one in which there exists no directing potential acting upon molecules, molecules may freely diffuse rotationally, and restrictions to translational diffusion occur on a length scale which is larger than the distance over which dipolar or quadrupolar couplings are significant [27] (the NMR timescale is shorter than the translational diffusion timescale). In solids, whether single crystals, stacked membranes or otherwise, relaxation is anisotropic. The precise form of the anisotropy depends on both the phase of matter and spin system, but in any of these cases, correlation functions retain angular dependence due to restricted motion. The spin interactions responsible for relaxation mechanisms are generally described by rank-2 tensor operators, hence orientation dependence is obvious. Coherence lifetime is invariably shorter than T2 due to inhomogeneous broadening since the dipolar Hamiltonian cannot be fully averaged to zero. Liquid crystals also have anisotropic relaxation times, the medium itself meaning motion is restricted [9, 33], for a directing potential is imposed.

Anisotropic NMR properties are well known *in vivo*, yet not fully understood, in certain biological tissues such as tendon and cartilage [10, 25], which plainly do not fulfil the criteria of isotropic liquids. T2 relaxation anisotropy scales in both tendon and cartilage according to the term $3\cos^2\theta-1$, T2 being longest at the fibre-to-field angle (θ) = 54.7°, i.e. at the magic angle. Anisotropy of coherence lifetime and T2* has also been observed in tendon [12, 23]. Anisotropic T1 of water protons has been observed in cartilage and tendon [7, 18], an angular dependency yet to be determined, however. Although it is clear that dipolar couplings between water protons are fundamental, it has yet to be resolved exactly how such anisotropy is mediated. There has been much recent interest in the anisotropy of coherence lifetime and T2 in the white matter (WM). The observation of T2* orientation dependence has led to the development of quantitative susceptibility mapping [11] and susceptibility tensor imaging [20]. However, in these methods, the anisotropy is of spin phase decoherence, not relaxation. Spin-echo coherence lifetime has also been shown to be anisotropic in the human WM [15, 17] and explained in terms of translational diffusion through inhomogeneous magnetic fields created by mesoscopic susceptibility differences [16]. The angular dependence of coherence lifetime anisotropy is such that T2 in WM follows a $\sin^4\theta$ dependency and is shortest at θ = 90° [15, 16].

T1-weigthed, often 3-dimensional MR, scans are commonly used for evaluation of brain morphometry including volumetry of either the entire brain or its substructures [5, 14]. The key factors that influence T1 relaxation time in the brain parenchyma are water, myelin and iron

content [31]. For instance, T1 relaxation time is longer in gray matter (GM) than in WM due to higher water and lower myelin content in the former tissue type than in the latter. Interestingly, a recent study indicated that WM microstructure may influence T1 relaxation rate in human brain [29]. In the present study we have examined a potential relationship between T1 relaxation time and fibre-to-field angle in human white matter at 3T, a relationship that has been established for T2 [17] and T2* [19] relaxation times.

2. METHODS

A total of 40 participants were recruited for this study (25 female, age range 23 to 71). They were required to have no known neurological disorder, past or present. All participants gave informed consent, and ethical approval was granted by the University of Bristol Faculty of Science Research Ethics Committee. All data were acquired using a Siemens Magnetom Skyra 3T system equipped with a 32-channel head coil, 2-channel parallel transmit body coil. The acquisition included a 3D T_1-weighted MPRAGE (sagittal, 0.86x0.86x0.86 mm^3), 2D multi-band diffusion tensor imaging (DTI) with 60 diffusion sensitising gradient directions [8] (axial, 1.88x1.88x1.98 mm^3), and a set of 3 MP2RAGE scans [22] (sagittal, 1.25x1.25x1.25 mm^3, TE 1.69 ms, total TR 1850 ms, TFL readout TR 4 ms, α 8°. A 10 ms hyperbolic secant pulse was used as the inversion pulse. The 6 TIs were 200, 300, 600, 900, 1200, and 1500 ms, where the inversion time defined as the time from the beginning of the inversion pulse to the phase encode centre line. Total scan time, including the localiser, was ~18 minutes.

Diffusion tensor images were computed using FSL version 5.06 (https://fsl.fmrib.ox.ac.uk/fsl/). Distortions caused by eddy currents were minimised using the program EDDY [3], and gross distortions due to interfaces between materials with different magnetic susceptibility corrected with the program TOPUP [2], prior to fitting diffusion tensors with DTIFIT. A single effective diffusion tensor was assumed for each voxel. T1 and S0 maps were fitted in Matlab (Mathworks, Natick, MA, USA) using one flip angle for the MP2RAGE data sets and assuming a single T1 time per voxel.

Fibre-to-field angle dependency of T1 was assessed using the method previously applied to anisotropy of coherence lifetime published [15, 17] to provide a heuristic demonstration as a surface plot of T1 as a function of FA and the angle θ (between the principal direction of diffusion and B_0). In this method, FA and θ are bin-ranged to create 2D bins of constant dimensions. All T1 observations falling into a bin are averaged. A surface plot may be thereby

produced. Data are required in a common space, chosen for each participant as that of their DTI data, re-sampled to 1 mm isotropic resolution. The relationship between fibre-to-field angle and S0 was determined in a similar fashion as for T1. Data in 4 distinct age ranges, each containing 10 of 40 participants, were pooled as motivated by the known age effect on WM microstructure and myelination, the so-called retrogenesis [28]. FSL FAST segmentation was used to segment GM, WM and CSF space. ROIs were manually drawn on the putamen, the head of caudate nucleus and lateral ventricles bilaterally using the multi-image analysis GUI routine (http://ric.uthscsa.edu/mango/) to measure average T1 values for each structure.

3. RESULTS

T1 values in various brain structures for the 4 age groups are shown (Table 1). T1 in CSF was 2904±680 ms. The numerical T1 values obtained by the MP2RAGE acquisitions, using shorter TR and higher flip angle in the GRE readout than those recommended for optimal T1 contrast [22], in Table 1 are in a close agreement to those reported at 3T except for the cortical GM. Long T1 for the GM reported here is likely to be due to partial voluming with CSF in GM voxels. Figure 1 shows histograms of the T1 in all WM voxels with diffusion FA ≥0.6 of the human brain according to the principal diffusion direction ("fibre-to-field" angle) identified by DTI. Where the principal diffusion direction is (nearly) parallel or perpendicular to B_0, T1 is broadly similar, but longer in the bin-range 50-60 degrees, which encompasses 'the magic angle'. Data are limited to an FA range of 0.6 or higher, 2.7% to 3.7% of all WM voxels falling within this FA range. It is evident that the margin by which T1 differs between "near-magic angle" WM structures and those far from the magic angle is similar to the overall T1 variation in WM over cohorts of 10 participants across age ranges of ~15 years. Typical T1 maps are shown next to each histogram panel.

Figure 2 shows the T1 on surface plots as a function of the fibre-to-field angle and FA of translational diffusion in the second dimension for all WM voxels. It is evident that the T1 angular dependence is present only at high FA, diminishing as FA reduces, with a near-flat T1 profile for FA < 0.3. The peak-to-trough distance for T1 at any given FA value appears to be larger in the younger age ranges (age groups 1 and 2) than the older (age group 4), such that T1 shows greater angular dependency in younger adult brains. S0 plots showed that the normalised S0 signal intensity was strongest in the fibre-to-field angle rage of 50-60° for voxel with FA >0.4 (Figure 3). S0s are elevated by 2-3% in all age groups 1-3 in the fibre-to-field angle rage of 50-60°, but somewhat less in the age group 4, although the shapes of the surface plots vary.

We next considered the possibility that the generally longer T1 around 'the magic angle' may be due to particular WM tracts having a preferential orientation around the magic angle and also having longer T1 conferred by anatomical properties. By examining the distribution of fibre-to-field angles in each tract and the density of near-magic angle orientations in each tract, we found this possibility to be unlikely, as shown in Figure 4. Although the thalamic superior longitudinal fasciculus (TSLoF) has a slightly higher density of near-magic angle fibre orientations, the TSLoF T1 is not generally higher across all angles. All tracts sample the angular range reasonably thoroughly, many with a 50-70° bias. Therefore, longer T1 around the magic angle is more probable to be an effect of fibre-to-field angle than anatomy.

4. DISCUSSION

We have observed what appears to be a "magic angle" effect in the T1 of the human WM in healthy adult participants, with T1 maximised around the magic angle of 54.7°. Our observation of angular dependency of T1 relaxation in human WM is in principle in agreement with a recent study showing that T1 relaxation rate is faster in fibres orienting perpendicularly to the B_0 [29]. However, both the exact fibre-to-field angle dependency and polarity of T1 change are much different in the study by Schyboll and co-workers to the current paper. Schyboll et al. acquired T1 data sets with (a) a two-point IR method with gradient echo readout and (b) an IR sequence with turbo-spin echo readout. Both T1 methods gave R1 versus fibre-to-field angle curves peaking around 30°- 40° with a plateau around 90°. The study by Schyboll and co-workers found an average T1 shortening of 2.6%, whereas we report an average lengthening of T1 by approximately 8%. Reasons for the discrepancies of observations remain unclear. However, a plausible explanation could be the different pulse sequences used for T1 measurements. We note that the measured T1 relaxation time in our study may have an additional confound in the form of a magnetisation transfer (MT) contribution. MT has been shown to contribute to the IR curve as measured by MP2RAGE resulting in bi-exponential recovery [32]. We used 6 TIs ranging from 200 to 1500 ms and found no evidence for bi-exponential T1 with any confidence. This may not, however, totally exclude the presence of more than one T1 component due to the choice of inversion pulse and/or TIs sampling the IR curve without short TIs (<200ms) [32]. While MT contribution remains a tenuous explanation for the T1 anisotropy observed in the WM, Henkelman et al. [13] reported in tendon 'deviation of MT curves as a function of B_0' resulting from the residual dipolar couplings of collagen and water protons. Any MT contribution to T1 would render the relaxation time sensitive to residual dipolar effects in myelin-associated water (short TE in MP2RAGE).

Our T1 results complement a growing body of evidence for strong influence of microstrcture on coherence lifetime [16], T2* [19, 34] and magnetic susceptibility [15] in the human brain in addition to well-established translational diffusion anisotropy [24, 30]. NMR relaxation times are governed by stochastic motions of the molecules including rotational diffusion, as well as internal molecular motions and translational diffusion, and are influenced by both the spin system and surroundings [1]. The measurement of relaxation times therefore provides molecular-scale information, as well as information on longer-range order and environment [21]. Relaxation occurs since stochastic motions randomly change the nuclear spin Hamiltonian, for example by changing dipolar couplings or chemical shift (or quadrupolar couplings for spins > ½), dissipating thermal energy and order from the system.

It is difficult to assign with confidence a single mechanism for the angular dependency of T1, though there are several candidates. Evidently our T1 observation is linked to microstructure of WM, because it is present only in WM with FA > 0.3 with fibre-to-field angle close to the magic angle. Both these DTI indices are robust measures of microstructural details, but they give no information regarding the detailed microstructure of axonal fibers. For instance, the FA range from 0.3 to 0.6 encompasses axons with greatly varying diameter [4]. Therefore, it is likely that the degree of structural anisotropy rather than finer microstructure of axon fibres imposes fibre-to-field dependent T1 relaxation. It also remains to be determined whether the effect is a direct observation of water protons, or protons of some other molecular species, or an exchange-mediated effect.

Fibre-to-field angle dependent T1 relaxation may be explained either by non-anisotropic or anisotropic mechanisms. In regard to non-anisotropic explanation a direct effect of water protons on T1 is a possibility, as MR-visible water content varies anatomically in WM [26, 35]. In addition to anatomical variation in water content, it was previously reported that MR-visible water may show a 'magic angle' type of effect such that it is elevated in WM fibres close to 55° with respect to the B_0 [29]. The study by Schyboll et al. analysed MR-visible water data using an advanced MRI protocol in total WM, segmented according to T1, without also analysing as a function of FA, and they reported that at fibre-to-field angles between 50° and 90° water content was approximately 0.6% greater than at 0° [29]. We also determined proton density (a proxy of MR-visible water) from the T1 fits and observed similar angular dependency of S0 in voxels with FA>0.4 as Schyboll et al. in WM globally. It would be tempting to conclude from the S0 plots and the MR-visible water data by Schyboll et al. [29] that the greater water

content in the WM tracts oriented close to magic angle with respect to the field would be behind the T1 anisotropy. However, in our study T1 and S0 are derived from the same fits of TI series data and can be interrelated due to a fitting bias, and potentially gaining contributions from other factors, such as dipolar couplings and/or immobile protons, as discussed below. Nevertheless, a working hypothesis that elevated non-anisotropically driven MR-visible water content underpins the observed angular dependency of T1 warrants further exploration.

In regard to anisotropic mechanisms, several candidates are identified. First, the non-water protons of the myelin sheath have an axis of alignment and are present in abundance in WM, especially where FA is high, in exactly these kinds of voxels where T1 anisotropy was seen. Therefore, the restricted motion (resulting in residual dipolar couplings) of non-water myelin sheath protons may be a contributor or sole cause. Protons of this nature are likely candidates for a 'semisolid pool' providing a vehicle for MT in WM. Second, water bound to, or in exchange with, the myelin sheath or axons also experiences restricted motion, such that the effect may be mediated by the myelin sheath but observed through water protons. A third possibility is that the folded layers of the myelin sheath creates an environment akin to nanocavities. Such an environment causes anisotropic relaxation since dipolar couplings cannot average to zero if the coordinates about a centre point are not equally probable (contrary to spherical cavities larger in diameter than the distance over which dipolar couplings are significant). Similar reasoning is invoked to explain translational diffusion anisotropy in the brain. Finally, the ordered myelin sheath, or some other factor, may create a directing potential acting upon water molecules in its vicinity such that the system behaves like a liquid crystal. Relaxation anisotropy is well known in such systems.

The question arises as to how the fibre-to-field angle dependency of T1 reported here relates to the observation of coherence lifetime [15]. The explanations proposed here, albeit qualitatively, all imply a T2 anisotropy which would be incorporated into coherence lifetime anisotropy measurements – and delineation may be challenging. However, the coherence lifetime anisotropy reports have invoked a model (and measurement protocol) in which the phenomenon is ascribed to translational diffusion distal to the myelin sheath, the anisotropy caused by magnetic field inhomogeneities [15, 16]. These are supposed to arise from the susceptibility difference between water and the myelin sheath itself. Therefore, angular dependency of T1 in WM may provide information complementary to coherence lifetime anisotropy, which may expand the combined use T1 relaxometry and DTI beyond solving the crossing fibre confounds in DTI [6].

Conclusions

We have provided evidence for fibre-to-field angle dependent T1 relaxation in the WM, and thus the encoding of microstructural information through T1 mapping by MRI. With an improved understanding of the source of angular dependency of T1, it may be possible to incorporate its measurement as a constraint on microstructural models, and therefore aid in extracting a greater level of information using quantitative MRI. We envisage that relaxometric MRI, incorporating T1 and T2, may also have an impact on the clinical diagnosis of diseases affecting WM microstructure, such as multiple sclerosis and strokes.

ACKNOWLEDGEMENTS

MJK was funded by the Elizabeth Blackwell Institute and by the Wellcome Trust international strategic support fund [ISSF2: 105612/Z/14/Z]. The work received support from the Dunhill Medical Trust [grant number R385/1114].

5. REFERENCES

1. A. Abragam, *Principles of Nuclear Magnetism*. international series of monographs on physics. 1961: Oxford Science Publications.
2. J.L. Andersson, S. Skare, and J. Ashburner, How to correct susceptibility distortions in spin-echo echo-planar images: application to diffusion tensor imaging. *Neuroimage*. **20**(2003): 870-88.
3. J.L. Andersson and S.N. Sotiropoulos, An integrated approach to correction for off-resonance effects and subject movement in diffusion MR imaging. *Neuroimage*. **125**(2016): 1063-78.
4. D. Barazany, P.J. Basser, and Y. Assaf, In vivo measurement of axon diameter distribution in the corpus callosum of rat brain. *Brain*. **132**(2009): 1210-20.
5. A.M. Dale, B. Fischl, and M.I. Sereno, Cortical surface-based analysis. I. Segmentation and surface reconstruction. *Neuroimage*. **9**(1999): 179-94.
6. S. De Santis, Y. Assaf, B. Jeurissen, D.K. Jones, and A. Roebroeck, T1 relaxometry of crossing fibres in the human brain. *Neuroimage*. **141**(2016): 133-42.
7. J. Du, B.C. Pak, R. Znamirowski, S. Statum, A. Takahashi, C.B. Chung, and G.M. Bydder, Magic angle effect in magnetic resonance imaging of the Achilles tendon and enthesis. *Magn Reson Imaging*. **27**(2009): 557-564.
8. D.A. Feinberg, S. Moeller, S.M. Smith, E. Auerbach, S. Ramanna, M. Gunther, M.F. Glasser, K.L. Miller, K. Ugurbil, and E. Yacoub, Multiplexed echo planar imaging for sub-second whole brain fMRI and fast diffusion imaging. *PLoS One*. **5**(2010): e15710.
9. J.H. Freed, Stochastic-molecular theory of spin–relaxation for liquid crystals. *J Chem Phys*. **66**(1977): 4183-4199.
10. G.D. Fullerton, I.L. Cameron, and V.A. Ord, Orientation of tendons in the magnetic-field and its effect on T2 relaxation-times. *Radiology*. **155**(1985): 433-435.
11. E.M. Haacke, S. Liu, S. Buch, W. Zheng, D. Wu, and Y. Ye, Quantitative susceptibility mapping: current status and future directions. *Magn Reson Imaging*. **33**(2015): 1-25.
12. R. Haken and B. Blümich, Anisotropy in tendon investigated in vivo by a portable NMR scanner, the NMR-MOUSE. *J Magn Reson*. **144**(2000): 195-199.
13. R.M. Henkelman, G.J. Stanisz, J.K. Kim, and M.J. Bronskill, Anisotropy of NMR Properties of Tissues. *Magn Reson Med*. **32**(1994): 592-601.
14. C.R. Jack, Jr., Alzheimer disease: new concepts on its neurobiology and the clinical role imaging will play. *Radiology*. **263**(2012): 344-61.

15. M.J. Knight, S. Dillon, L. Jarutyte, and R.A. Kauppinen, Magnetic resonance relaxation anisotropy: Physical principles and uses in microstructure imaging. *Biophys J*. **112**(2017): 1517-1528.
16. M.J. Knight and R.A. Kauppinen, Diffusion-mediated nuclear spin phase decoherence in cylindrically porous materials. *J Magn Reson*. **269**(2016): 1-12.
17. M.J. Knight, B. Wood, E. Coulthard, and R.A. Kauppinen, Anisotropy of spin-echo T2 relaxation by magnetic resonance imaging in the human brain in vivo. *Biomed Spectr Imag*. **4**(2015): 299-310.
18. L.V. Krasnosselskaia, G.D. Fullerton, S.J. Dodd, and I.L. Cameron, Water in tendon: Orientational analysis of the free induction decay. *Magn Reson Med*. **54**(2005): 280-288.
19. J. Lee, P. van Gelderen, L.W. Kuo, H. Merkle, A.C. Silva, and J.H. Duyn, T2*-based fiber orientation mapping. *Neuroimage*. **57**(2011): 225-234.
20. X. Li, D.S. Vikram, I.A.L. Lim, C.K. Jones, J.A.D. Farrell, and P.C.M. van Zijl, Mapping magnetic susceptibility anisotropies of white matter in vivo in the human brain at 7 T. *NeuroImage*. **62**(2012): 314-330.
21. P. Luginbühl and K. Wüthrich, Semi-classical nuclear spin relaxation theory revisited for use with biological macromolecules. *Prog Nucl Magn Reson Spectrosc*. **40**(2002): 199-247.
22. J.P. Marques, T. Kober, G. Krueger, W. van der Zwaag, P.F. Van de Moortele, and R. Gruetter, MP2RAGE, a self bias-field corrected sequence for improved segmentation and T1-mapping at high field. *Neuroimage*. **49**(2010): 1271-81.
23. K.I. Momot, J.M. Pope, and R.M. Wellard, Anisotropy of spin relaxation of water protons in cartilage and tendon. *NMR Biomed*. **23**(2010): 313-24.
24. M.E. Moseley, Y. Cohen, J. Kucharczyk, J. Mintorovitch, H.S. Asgari, M.F. Wendland, J. Tsuruda, and D. Norman, Diffusion-weighted MR imaging of anisotropic water diffusion in cat central nervous system. *Radiology*. **176**(1990): 439-45.
25. G. Navon, U. Eliav, D.E. Demco, and B. Blümich, Study of order and dynamic processes in tendon by NMR and MRI. *J Magn Reson Imaging*. **25**(2007): 362-380.
26. H. Neeb, V. Ermer, T. Stocker, and N.J. Shah, Fast quantitative mapping of absolute water content with full brain coverage. *Neuroimage*. **42**(2008): 1094-109.
27. M.P. Nicholas, E. Eryilmaz, F. Ferrage, D. Cowburn, and R. Ghose, Nuclear spin relaxation in isotropic and anisotropic media. *Prog Nucl Magn Reson Spectr*. **57**(2010): 111-58.
28. B. Reisberg, E.H. Franssen, L.E. Souren, S.R. Auer, I. Akram, and S. Kenowsky, Evidence and mechanisms of retrogenesis in Alzheimer's and other dementias:

management and treatment import. *Am J Alzheimers Dis Other Demen*. **17**(2002): 202-12.

29. F. Schyboll, U. Jaekel, B. Weber, and H. Neeb, The impact of fibre orientation on T1-relaxation and apparent tissue water content in white matter. *MAGMA*. **31**(2018): 501-510.
30. C. Thompsen, O. Hendriksen, and P. Ring, In vivo measurement of water self diffusion in the human brain by magnetic resonance imaging. *Acta Radiol Scand*. **28**(1987): 353-361.
31. P. Tofts, *Quantitative MRI of the Brain: Measuring Changes Caused by Disease*. 2004, Chichester, England: John Wiley& Sons, Ltd.
32. P. van Gelderen, X. Jiang, and J.H. Duyn, Effects of magnetization transfer on T1 contrast in human brain white matter. *Neuroimage*. **128**(2016): 85-95.
33. R.R. Vold and R.L. Vold, Nuclear spin relaxation and molecular dynamics in ordered systems: Models for molecular reorientation in thermotropic liquid crystals. *J Chem Phys*. **88**(1988): 1443-1457.
34. S. Wharton and R. Bowtell, Fiber orientation-dependent white matter contrast in gradient echo MRI. *Proc Natl Acad Sci USA*. **109**(2012): 18559-18564.
35. K.P. Whittall, A.L. MacKay, D.A. Graeb, R.A. Nugent, D.K. Li, and D.W. Paty, In vivo measurement of T2 distributions and water contents in normal human brain. *Magn Reson Med*. **37**(1997): 34-43.

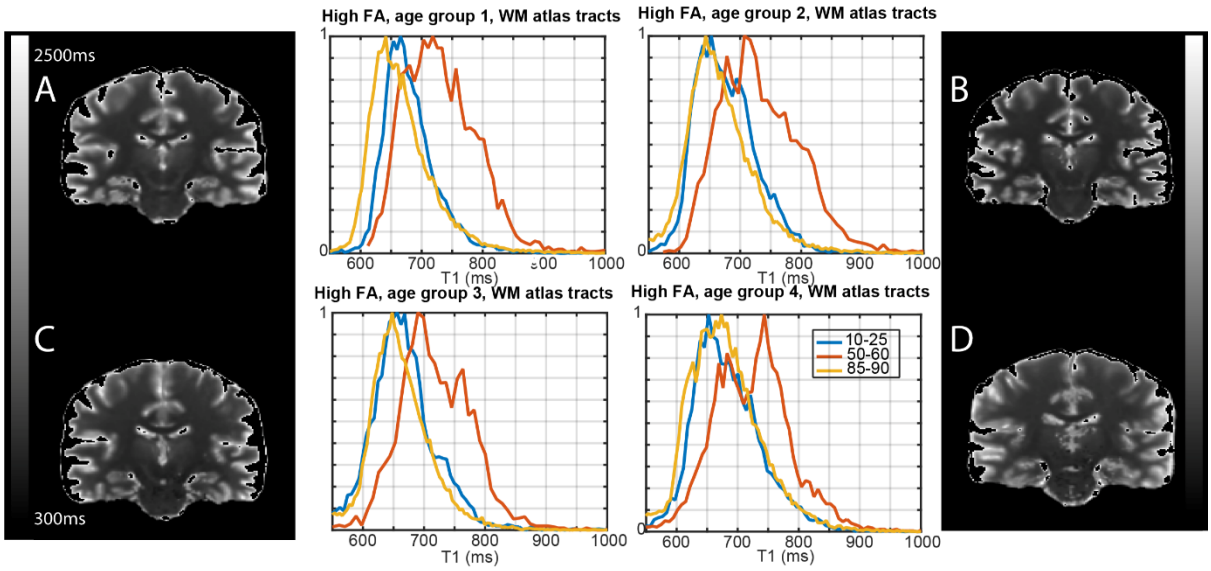

Figure 1: Histograms of white matter T1 in four different age groups, and three different angular bin ranges with representative coronal T1 maps. Age groups are as follows: 1 from 23 to 33 (A is the representative T1 map); 2 from 33 to 48 (B is the representative T1 map); 3 from 48 to 60 (C is the representative T1 map) and 4 from 60 to 72 years (D is the representative T1 map). The legend refers to the angular bin range (10°-25°; 50°-60° and 85°-90°), denoting the range of "fibre-to-field" angles (derived from DTI) in which data were pooled. Voxel-wise data were restricted to voxels with FA higher than 0.6 (referred to as 'high FA'). Number of voxels were as follows: group 1 (10°-25°) 15,081, (50°-60°) 6,982, (85°-90°) 33,615; group 2 (10°-25°) 9,541, (50°-60°) 4,942, (85°-90°) 26,828; group 3 (10°-25°) 12,417, (50°-60°) 4,209, (85°-90°) 26,753; group 4 (10°-25°) 11,380, (50°-60°) 5,274, (85°-90°) 20,569. In T1 maps voxels with T1>3,000 ms are zeroed, T1 scale bar is in ms.

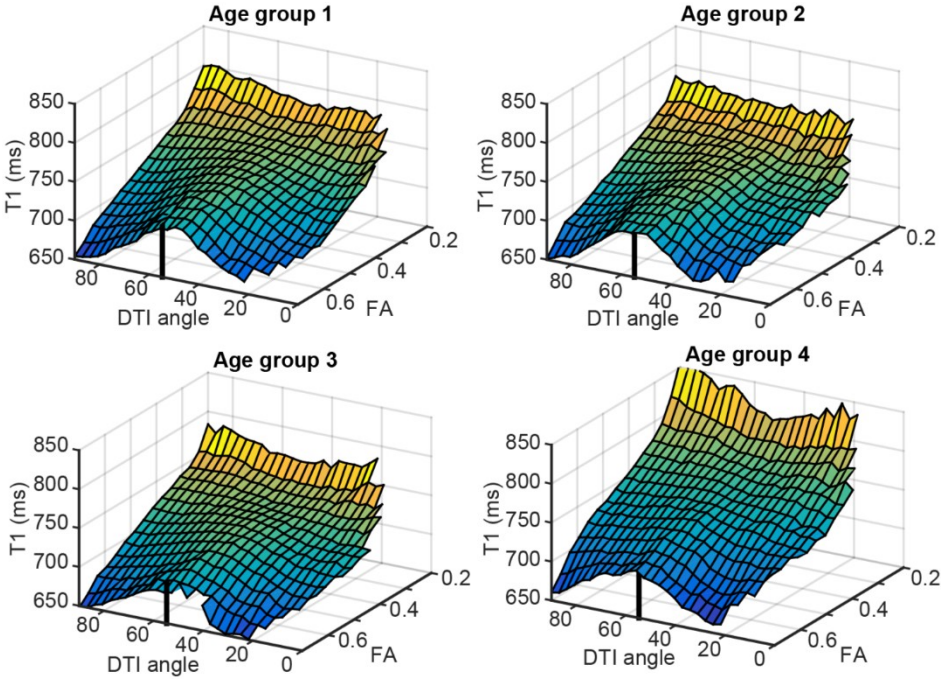

Figure 2: Surface plots of T1 as a function of fibre-to-field angle and FA in four age ranges. Each point on a surface represents the median T1 of all WM data in the age group falling in the corresponding 2D [angle, FA] 2D bin. The magic angle is indicated with a solid black line. Age groups as defined in the legend to Figure 1.

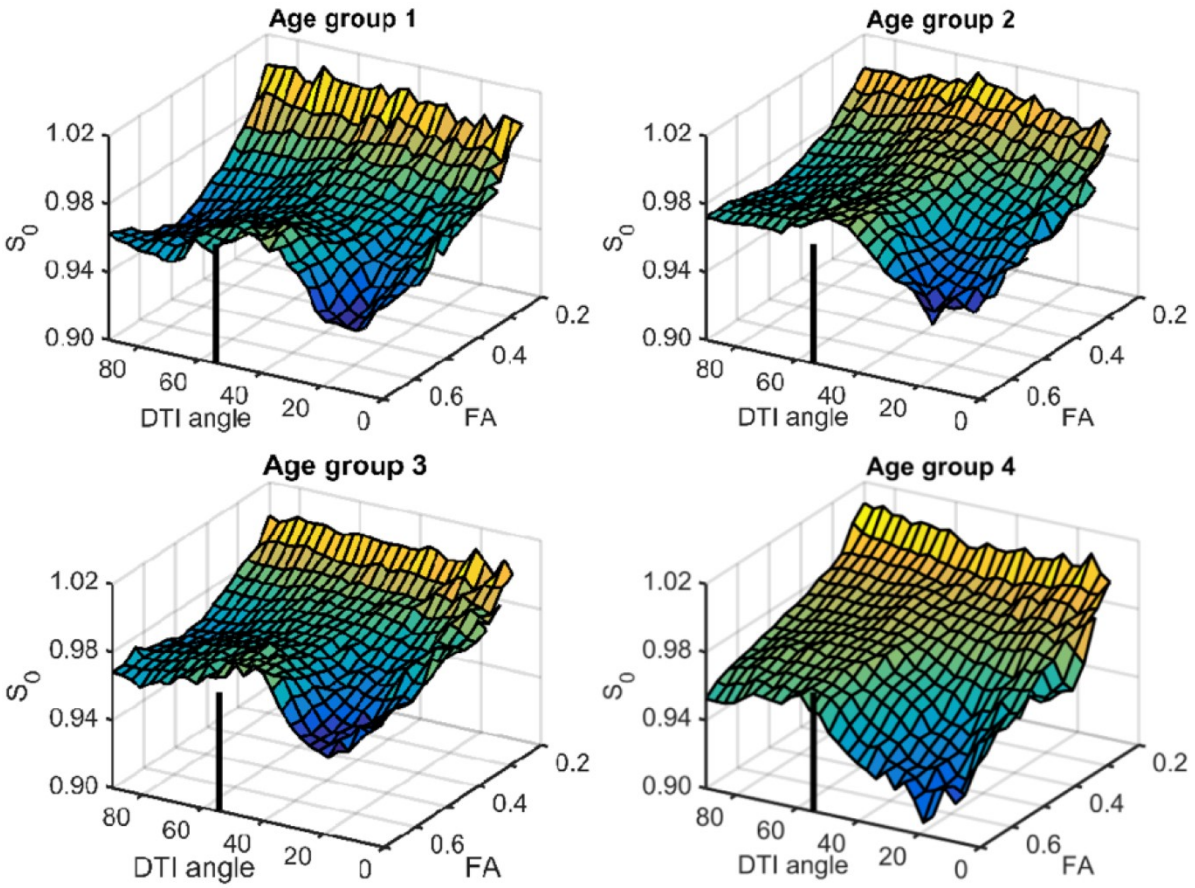

Figure 3: Surface plots of S0 as a function of fibre-to-field angle and FA in four age ranges.

S0 maps were normalised using the averaged values from voxels with FA=0.2 as reference, because T1 in these voxels showed no angular dependency. Magic angle is marked with a solid black line, age groups as in Figure 1.

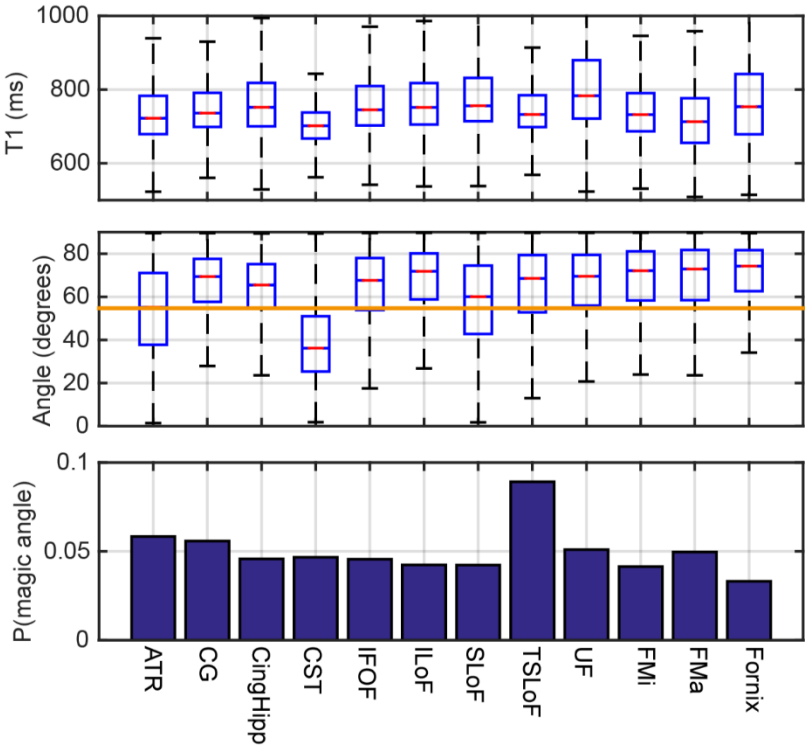

Figure 4: Boxplot representations of T1 and directional distributions, and density of magic-angle directional observations by tract. The boxplots were calculated over the entire cohort of 40 participants. The bar plot shows the probability of observing a principal diffusion direction within +/- 5 degrees of the magic angle in each tract of the JHU atlas normalised by tract, such that the maximum value in each tract is 1. ATR = anterior thalamic radiation; CG = corpus callosum; CingHipp = cingulum in hippocampus; CST = cortico-spinal tract; IFOF = inferior fronto-occipital fasciculus; ILoF = inferior longitudinal fasciculus; SloF = superior longitudinal fasciculus; TSLoF = thalamic superior longitudinal fasciculus; UF = uncinate fasciculus; FMi = forceps minor; FMa = forceps major.

Table 1. T1 values in human brain at 3T.

Tissue type	**Age group 1**	**Age group 2**	**Age group 3**	**Age group 4**
Cortical GM	1703±102	1598±132	1610±114	1672±95
Putamen	953±41	946±44	920±58	967±58
Caudate nucleus	1149±118	1129±82	1094±36	1145±102
WM	885±37	866±26	867±27	936±37

T1 values (in milliseconds, mean ± SD) are given for each specified brain structure for the four age groups as follows: Age group 1 (from23 to 33 years of age), Age group 2 (from 33 to 48 years), Age group 3 (from 48 to 60 years) and Age group 4 (from 60 to 72 years).